

ChewBaccaNN: A Flexible 223 TOPS/W BNN Accelerator

Renzo Andri^{§*}, Geethan Karunaratne^{*†}, Lukas Cavigelli^{§*}, Luca Benini^{*‡}

^{*}Integrated Systems Laboratory, ETH Zurich, Zurich, Switzerland [†]IBM Research, Zurich, Switzerland

[§]Huawei Technologies, Zurich Research Center, Zurich, Switzerland [‡]DEI, University of Bologna, Bologna, Italy

Abstract—Binary Neural Networks enable smart IoT devices, as they significantly reduce the required memory footprint and computational complexity while retaining a high network performance and flexibility. This paper presents ChewBaccaNN, a 0.7 mm² sized binary convolutional neural network (CNN) accelerator designed in GlobalFoundries 22 nm technology. By exploiting efficient data re-use, data buffering, latch-based memories, and voltage scaling, a throughput of 241 GOPS is achieved while consuming just 1.1 mW at 0.4V/154MHz during inference of binary CNNs with up to 7×7 kernels, leading to a peak core energy efficiency of 223 TOPS/W. ChewBaccaNN’s flexibility allows to run a much wider range of binary CNNs than other accelerators, drastically improving the accuracy-energy trade-off beyond what can be captured by the TOPS/W metric. In fact, it can perform CIFAR-10 inference at 86.8% accuracy with merely 1.3 μJ, thus exceeding the accuracy while at the same time lowering the energy cost by 2.8× compared to even the most efficient and much larger analog processing-in-memory devices, while keeping the flexibility of running larger CNNs for higher accuracy when needed. It also runs a binary ResNet-18 trained on the 1000-class ILSVRC dataset and improves the energy efficiency by 4.4× over accelerators of similar flexibility. Furthermore, it can perform inference on a binarized ResNet-18 trained with 8-bases Group-Net to achieve a 67.5% Top-1 accuracy with only 3.0 mJ/frame—at an accuracy drop of merely 1.8% from the full-precision ResNet-18.

Keywords—Binary Neural Networks, Hardware Acceleration

I. INTRODUCTION

CNNs have revolutionized the ML field in recent years, outperforming humans in image recognition [1] and advancing the SoA for a wide range of applications [2]. Most of these networks require billions of multiply-accumulate (MAC) operations per frame and millions of trained parameters. This is incompatible with the few hundreds of kB of on-chip memory and the limited energy available on battery-powered, low-cost IoT sensor nodes.

Sending the data to the cloud for analysis seems like a viable option to forego these challenges. However, transmitting the data comes at a high energy cost, introduces privacy concerns, requires expensive infrastructure, and has high latency. Alternatively, the challenge of analyzing the data near the sensor can be tackled by a combination of algorithmic optimizations to allow working with reduced arithmetic precision, and hardware acceleration [3], [4] with various techniques

maximize energy efficiency, such as minimizing off-accelerator data transfers [5]–[7].

Reducing the arithmetic precision has shown significant potential, affecting both the complexity of the compute operation itself as well as reducing data movement and storage requirements for the feature maps and the weights.

Inference with 8 bit operands has become common-place due to the negligible accuracy loss for many applications with support available in many deep learning frameworks and commercial hardware [8].

At the extreme limit, binarized neural networks (BNNs) quantize weights and feature maps to a single bit representing the values -1 and 1. XNOR-Net extends the stochastic gradient descent algorithm (commonly used to train NNs) by quantizing the weights and activations in the forward path and scales the feature maps ℓ^1 matrix norm of the weight kernels [9]. On the challenging ImageNet dataset, Rastegari et al. achieved 51.2% using a binarized ResNet-18, which was a significant drop of -18.1%. Courbariaux et al. achieved then SoA results with 99.04% on MNIST (+0.34%), 97.47 on SVHN (-0.09%), and 89.85% CIFAR-10 (-0.46%), but these datasets are much simpler than ImageNet [10].

Recent research has been focusing mainly on minimizing the quantization error (e.g., scaling feature maps in XNOR-Net), improving the loss function, and reducing the gradient error [11], [12]. Recently, the accuracy gap between BNNs and their full-precision equivalents have been brought down to 12% (DoReFa-Net on Alexnet [13]) and can be reduced by using multiple binary layers (i.e., weight bases) in parallel and binarizing around multiple thresholds (i.e., activation bases). Using 3 weight bases, Lin et al. [14] have achieved 69.3%/89.2% (Top-1/Top-5, -8.3%/-6.0% vs. ResNet-18) and Zhuang et al. reached 72.8%/90.5 (Top-1/Top-5, -3.2%/-2.4% vs. ResNet-50) using 8 weight bases [15]. Using multiple bases directly impacts the throughput and energy per inference for any hardware accelerator, negating some of the benefits of BNNs. However, it enables smoothly scaling from a highly efficient, less accurate network to almost full accuracy inference.

BNN hardware accelerators have demonstrated around two orders of magnitude energy efficiency gain compared to quantized NN accelerators by avoiding off-chip data transfers and exploiting extremely reduced arithmetics where a MAC becomes binary *xnor*-popcount. Conti et al. present a 46 TOPS/W BNN accelerator tightly-connected to a general-purpose processor (omitting I/O costs) [16], UNPU is a stand-alone accelerator for flexible weights (i.e., 1-16 bit) and feature maps and reaches 51 TOPS/W for fully-binary NN [17]. Furthermore, accelerators with fixed and uncommon kernel sizes 2 × 2 [18], [19] and analog computation [18], [20] show a theoretic peak energy efficiency of 866 TOPS/W, but lack

©2021 IEEE. Personal use of this material is permitted. Permission from IEEE must be obtained for all other uses, in any current or future media, including reprinting/republishing this material for advertising or promotional purposes, creating new collective works, for resale or redistribution to servers or lists, or reuse of any copyrighted component of this work in other works.

IEEE ISCAS 2021, Daegu, South Korea, 23–26 May 2021

DOI: TBD

URL: <http://ieeexplore.ieee.org/document/TBD/>

flexibility and require significant larger BNNs for competitive network performance.

In this paper, we present ChewBaccaNN, an enhanced architecture and novel implementation based on XNORBIN [21], increasing the energy efficiency by $2.3\times$ through a redesign of the memory architecture including a switch to latch-based memories to allow more aggressive voltage scaling down to 0.4V and adjusted memory sizes to eliminate off-chip storage of intermediate results, as well as enhanced power gating to dynamically turn off unused memory banks, and a more advanced technology node. Combining these methods, we achieve an energy efficiency of 223 TOPS/W with a fully-digital accelerator in 22 nm. New features, including support for average pooling and residual paths, dramatically boost the accuracy-energy trade-off beyond the scope of the TOPS/W metric, allowing us to run inference at 91.5% accuracy with 7.3 μ J or 86.8% with 1.3 μ J on CIFAR-10—an improvement of $2.8\times$ over the state-of-the-art.

II. BNN AND RELATED HW OPTIMIZATION

In BNNs, the weights and intermediate feature maps are quantized to a single bit: $\mathbf{I} \in \{-1, 1\}^{n_{in} \times i_h \times i_w}$ $\mathbf{W} \in \{-1, 1\}^{n_{out} \times n_{in} \times h_k \times w_k}$, with spatial feature map size of $i_h \times i_w$, kernel size $h_k \times w_k$ and number of input/output channels n_{in} , n_{out} . After the multiplication, which is reduced to an xnor operation, these products and a bias value are accumulated in full-precision followed by re-binarizing the sum. This (re-)binarization replaces the activation function and has the behavior of a signum function while zero is mapped to 1, i.e., $\forall x > 0 : \text{sgn}(x) = 1$ and $\forall x \leq 0 : \text{sgn}(x) = -1$. The ℓ -th output feature map \mathbf{o}_ℓ is the sum of convolutions of every binarized input feature map \mathbf{i}_n with the corresponding binary weights $\mathbf{w}_{\ell,n}$ and the bias C_ℓ :

$$\mathbf{o}_\ell = \text{sgn} \left(C_\ell + \alpha_\ell \sum_{n=0}^{n_{in}-1} \text{sgn}(\mathbf{i}_n) * \text{sgn}(\mathbf{w}_{\ell,n}) \right) \quad (1)$$

BNNs have much potential for optimizations: First, the memory footprint can be reduced up to $32\times$ (relative to FP32). Second, multiplications can be simplified to xnor operations. Training of BNNs is not trivial, as signum function is not smooth and thus not differentiable. The most common approach, known as straight-through estimator, is based on shadow weights in high precision (e.g., FP32) [22]. These weights are binarized during the forward-propagation while during back-propagation, the gradients are passed on to the input as without quantization and the gradient update is applied to the shadow weights. Typically, the weights of the first and last layers are not binarized, as this has a strong impact on the network performance, but contributes a small part of the total compute effort [13].

For implementation, the bipolar activations and weights $i_n, w_{\ell,n} \in \{-1, 1\}$ are mapped to the binary representation $\hat{i}_n, \hat{w}_{\ell,n} \in \{0, 1\}$ with $\hat{x} = \frac{1}{2}(x+1)$, enabling the replacement of the multiplication with a xnor operation. This introduces an offset ($-h_k w_k$) and scaling factor (2) that need to be applied before the re-binarization:

$$\mathbf{o}_\ell = \text{sgn} \left(C_\ell + \alpha_\ell \sum_{n=0}^{n_{in}-1} \left(2 \cdot \hat{\mathbf{i}}_n *^{\oplus} \hat{\mathbf{w}}_{\ell,n} - h_k w_k \right) \right)$$

The factor and offset of the BNN convolution, C_ℓ , α_ℓ , and the parameters μ_ℓ , σ_ℓ of the following batch normalization layer can be absorbed into single threshold $\theta_\ell = \frac{C_\ell \sigma_\ell}{|\alpha_\ell|} + \mu_\ell$, applied to the sum of products,

$$\mathbf{o}_\ell = \begin{cases} -1, & \sum_{n=0}^{n_{in}-1} \hat{\mathbf{i}}_n *^{\oplus} \hat{\mathbf{w}}_{\ell,n} < \theta_\ell \\ 1, & \text{else} \end{cases} \quad (2)$$

Pooling is applied after convolution, scaling, and batch normalization, but before the re-binarization, therefore, in the non-binary domain. However, due to the monotonicity and commutativity, the pooling can be calculated as a Boolean operation (e.g., max/min-pooling becomes AND/OR reduction).

III. ARCHITECTURE

The architecture of ChewBaccaNN is illustrated in Fig. 1a and its components are explained as follows:

Each *Basic Processing Unit (BPU)* performs a 1D convolution of an input image row with a kernel row from 16 input channels at a time, by employing *xnor_sum* units consisting of 16 *xnor*-gates each and a popcount adder tree. The *xnor_sum* unit is replicated 7 times to produce outputs corresponding to a window size of at most 7 input feature map pixels in a row. Outputs from all units are accumulated together with a second stage adder tree to create a 1D inner product, shown in Fig. 1b). 7 BPUs form the BPU array, instantiated in order to support kernel sizes up to 7×7 . The outputs of all these instances are pipelined to increase throughput and are then added up in a third stage adder tree to produce 2D inner product. Each of the *xnor*-sum instances is fed with the input activations and weight data through a controlled shift-register to enable data reuse. The same BPU array datapath is reused to perform binary max-pooling operation, where the 2nd and 3rd stage adder trees are flanked by a 1 bit comparator (AND gate) tree. ChewBaccaNN comes with a *Feature Map Memory FMM* and data buffering.

The FMM stores the feature maps and the partial sums of the convolutions. The memory is divided into two blocks, where one serves as the data source (i.e., current input feature maps), and the other serves as data sink (i.e., partial or final output feature maps). They are swapped after each layer. If the FMM is dimensioned to fit the largest intermediate FMs, no energy-costly off-chip memory accesses are needed during inference. To hide the weight loading latency, the PB is enriched with a double buffering feature. The *Parameter Buffer PB* stores the weights, the binarization thresholds, and the configuration parameters. In the optimal case, it stores all the weights of the network to avoid I/O for weight loading. If the parameters are too many to fit on-chip, the PB can be reused to buffer off-chip accesses. The *Row Banks* are used to buffer rows of the input feature maps for frequent accesses. It also contains rows of filter weights corresponding to the batch of output channels calculated in parallel. Since these row banks need to be rotated when shifting the convolution window down, they are connected to the BPU array through a crossbar.

The crossbar connects the registers inside the BPUs, the *controlled shift registers (L1) (CSRs)* containing kernel input feature map elements, and the filter weight elements. These are shifted when the convolution window is moved forward. The *DMA* moves data independently from FMM and PB into (via

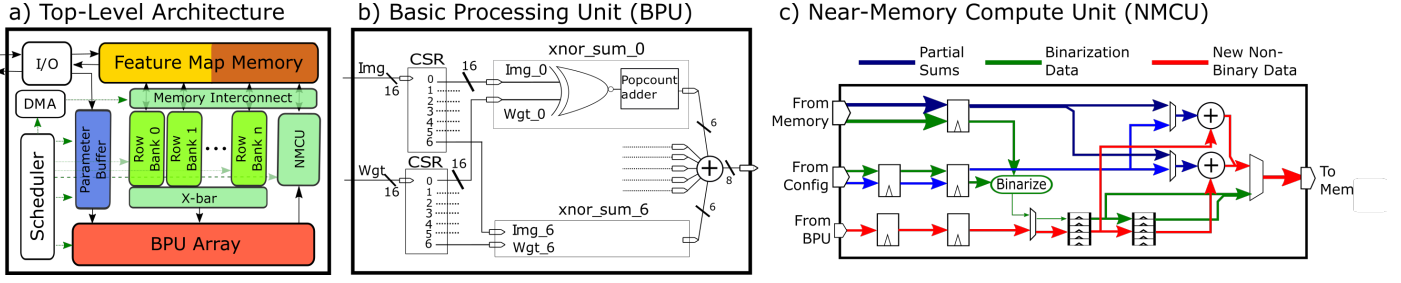


Fig. 1: Architecture overview. a) Top-level schematic, b) Detailed schem. of a single BPU, c) Detailed schem. of near-memory compute unit.

Row Banks) and out of the BPU array. *Scheduler*: According to the layer configuration of a CNN, the scheduler controls the crossbar on how and when to route feature map and weight data from the Row Banks to the BPUs in order to compute row-wise partial sums for each member in the batch. The *Near Memory Compute Unit (NMCU)* is shown in Fig. 1c and is used for on-the-fly computation when writing back to the FFM. This includes partial sum calculations from the BPU array, accumulating residual paths from the FMM, the binarization, and storing in FFM in a packed format (i.e., 16 activations).

To maximize kernel-level reuse, filter weights are retained in BPUs while streaming selected image rows through BPUs, and partial sums are computed concurrently for a batch of output feature map tile to maximize row-level image reuse. The resulting integer value that is produced from the BPU array in each cycle as a result of a horizontally sliding convolution window is forwarded to the DMA controller via the *Near-Memory Compute Unit (NMCU)*. The NMCU accumulates the partial results by means of a read-add-write operation. After the final accumulation of partial results, the unit also performs the thresholding/re-binarization operation (i.e., activation and batch normalization). The binary results are packed into 16 bit words and written back to the memory by the DMA unit. The scheduling is determined with the objective of maximizing the data reuse at different levels of the memory hierarchy.

The scheduling algorithm and mapping of operations to BPU units are explained in Alg. 1 based on the filter dimensions k_w and k_h , the spatial input dimensions i_w and i_h , the depths (i.e., input channels c_i , and output channels c_o) and the channels tile sizes \hat{c}_i and \hat{c}_o . Parallel execution is indicated in the brackets in lines 4, 6—8. After one tile of output channels \hat{c}_o is computed (i.e., binary convolution, (optional) pooling and thresholding), the process is repeated for all output channel tiles. In the next step, the next subsequent layer with new layer configuration is loaded, the FMM sink/source direction is reversed, and calculated.

IV. RESULTS & DISCUSSION

A. Physical Implementation

ChewBaccaNN has been implemented in GlobalFoundries 22nm FDX (7.5T). To reach the highest energy efficiency, we operate at $V_{DD}=0.4V$ with 0.1V forward body-biasing. To scale the voltage down to this level and to reduce the energy cost per memory access by $3.5\times$, we use standard-cell memories (SCMs) instead of SRAMs. They are designed with hierarchical clock gating and address/data silencing mechanisms, thus when a bank is not accessed the whole latch array consumes no dynamic power [4]. The SCMs are composed

Algorithm 1 High-level scheduling of 1 BNN layer

Require: $k_w, k_h, i_w, i_h, c_i, c_o, \hat{c}_i, \hat{c}_o$

- 1: **for** $n_o \leftarrow 0$ **to** c_o/\hat{c}_o **do**
- 2: **for** $n_i \leftarrow 0$ **to** c_i/\hat{c}_i **do**
- 3: pass n_i^{th} chunk of next \hat{c}_o filters to Row Banks
- 4: **for** $n_r \leftarrow 0$ **to** i_h **do**
- 5: pass Feature Map $(:, n_r, n_i * b_i : + b_i)$ to Row Banks
- 6: **for** $b_o \leftarrow 0$ **to** \hat{c}_o **do**
- 7: pass n_i^{th} chunk of b_o^{th} filter to BPU array
- 8: **for** $n_c \leftarrow 0$ **to** i_w **do**
- 9: pass Feature Map $(n_c, n_r + k_r, n_i * b_i : + b_i)$ to BPU array
- 10: **for** $k_r \leftarrow -(k_h/2)$ **to** $(k_h/2)$ (parallel in BPU array) **do**
- 11: **for** $k_c \leftarrow -(k_w/2)$ **to** $(k_w/2)$ (parallel in BPU) **do**
- 12: **for** $b_i \leftarrow 0$ **to** \hat{c}_i (parallel in BPU gates) **do**
- 13: Produce Partial Sum $(n_c, n_r, \hat{c}_o * n_o + b_o)$ at NMCU
- 14: Accumulate Partial Sum $(n_c, n_r, \hat{c}_o * n_o + b_o)$ at NMCU
- 15: Binarize final Partial Sum $(:, n_i * \hat{c}_i : + \hat{c}_i)$
- 16: Pool operation (if applicable)

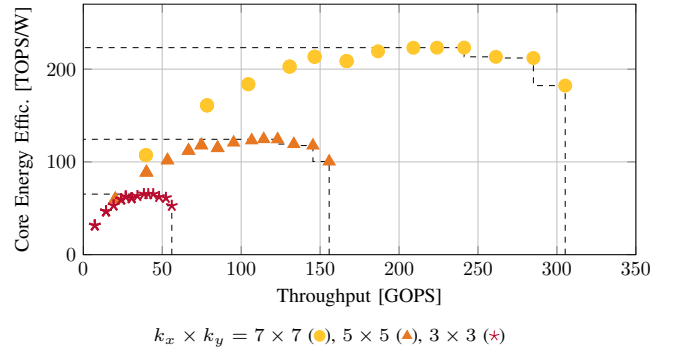


Fig. 2: Throughput vs. Core Energy Efficiency for various timing constraints at 0.4V supply voltage and FMM=4kB.

of multiple banks of $256 \text{ words} \times 32 \text{ bit}$ (1kB). The FMM is dimensioned to fit the two largest consecutive layers of the network, which has to be supported without tiling. We have selected them to be either 16 and 32 SCM banks (48 kB) for AlexNet or 2×73 banks (146 kB) for both AlexNet and ResNet-18; the parameter buffer has 2 banks (3.5 kB) and the 7 row bank memories consist of 1 SCM bank each (i.e., 3.5 kB in total). The final floorplan is shown in Fig. 3. It can be seen that a large part of the chip (i.e., 97%) are memories, whereas the compute units just occupy 1% of the total chip area of 0.7 mm^2 . The power consumption has been evaluated with back-annotated post-layout simulation with stimuli generated from a pretrained Torch model. I/O energy has been estimated with 21 pJ/bit (LPDDR3 memory access cost [5]).

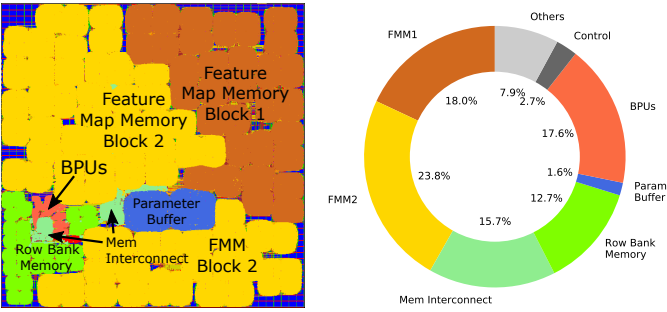


Fig. 3: Floorplan and power breakdown of ChewBaccaNN core

B. Throughput to Energy Efficiency Trade-Off

We have synthesized and run back-ends at various timing constraints, to explore the energy-efficiency to throughput trade-off at 0.4 V, shown in Fig. 2. Due to the lower density of the SCM memories compared to SRAMs, the chip reports high leakage, which limits the core energy efficiency to 185/100/39.0 TOPS/W (for the full-utilization case of $7^2/5^2/3^2$ kernel sizes) with 48 kB FMM (i.e., same size as XNORBIN) at a throughput of 241/123/44.3 GOPS and a core power consumption of 1.3/1.2/0.90 mW, where the power consumption can be broken down as shown in Fig. 3 in 56.1% memory, 15.7% memory interconnects and buffers, 17.6% compute units, 2.7% control, and 7.9% others. Fortunately, most of the FMM banks stay unused and can, therefore, be power-gated. Thus, with 4 active banks (4 kB) the energy consumption reduces to 1.08/0.99/0.68 mW and the energy efficiency can be increased up to 223/124/65 TOPS/W. Tab. I provides an overview of SoA BNN accelerators: the strongest analog [18], analog-in-memory [20], and digital accelerators [17], [19], [23]. Among the digital accelerators, UNPU is the only one supporting commonly used 3×3 and 5×5 kernels, while the others rely on 2×2 kernels. Therefore, ChewBaccaNN shows a $2.0 \times$ better energy-efficient compared to flexible SoA BNN accelerators [17]. For 7×7 kernels ChewBaccaNN outperforms UNPU even $4.4 \times$. Even though the other accelerators show a very high energy efficiency, up to 866 TOPS/W compared to 36 TOPS/W sustained energy efficiency for Rusci et al. [24], ChewBaccaNN still outperforms the SoA by $2.8 \times$ in energy per classification for CIFAR-10 while achieving similar accuracies. The main reason is that they rely on uncommon 2×2 kernels and have to compensate for process and ambient variations in the analog accelerators, and therefore require computationally significantly more complex networks (i.e., up to $51 \times$). A significant improvement in accuracy can be achieved on ChewBaccaNN by using IR-Net from Qin et al. [25], which achieves 91.5% accuracy at 7.3 μ J per inference.

C. Accuracy and Energy-Efficiency for Various BNNs

In this section, we compare the state-of-the-art of BNNs and how efficiently they map to ChewBaccaNN in Tab. II. The networks are pretrained and there is no accuracy drop when mapping to ChewBaccaNN due to its bit-true mapping of BNNs. The first two BNNs have been used in embedded applications. Cerutti et al. presented a BNN for Sound Event Detection on the Freesound database with 28 classes [26]. The audio data is converted to a Mel-frequency cepstral spectrogram and fed to a binary CNN with 5 layers with

TABLE I: Comparison with SoA Accelerators. ChewBaccaNN performing CIFAR-10 with: Rusci et al. [24]/IR-Net [25]

Accelerator	[20]	[18]	[17]	[23]	[19]	OURS
Digital/Analog	Analog/PIM	Analog	Digital	Digital	Digital	Digital
Tech. Node [nm]	65	28	65	28	10	22
Area [mm ²]	12.6	4.6	16	1.4	0.39	0.7
MemCap [kB]	295	328	256	328	161	153
Voltage [V]	0.68	0.60	0.63	0.66	0.37	0.40
Power [mW]	22	0.094	3.2	1.5	5.6	1.1
Peak Throughput [TOPS]	19	0.072	0.18	0.35	3.4	0.24
Peak Efficiency [TOPS/W]	866	772	51	230	617	223
Kernel Support	3^2	2^2	$3^2, 5^2$	2^2	2^2	$1^2, 3^2, 5^2, 7^2$
Network	[20]	[23]	-	[23]	[23]	[24] / [25]
Accuracy CIFAR-10 [%]	83.27	86.05	-	86.05	86.05	86.8 / 91.5
Net Size [MOp]	2'340	2'016	-	2'016	2'016	46 / 175
Energy/Inference [μ J]	3.6	3.8	-	14.4	5.2	1.3 / 7.3

3×3 kernels, followed by 3 layers with 1×1 kernels. They achieve a 77.9% accuracy (i.e., a drop of 7.9% with respect to full-precision). Rusci et al. trained and implemented a VGG-like network on the CIFAR-10 dataset which does image recognition on 32×32 colored images with 10 classes, and achieves an accuracy of 86.6% (4.6% less than FP32 baseline) [24]. Both networks have been implemented on the low-power Gapuino board featuring the GAP8 multi-core processor, with 8+1 energy-optimized RISC-V cores implementing the RISC-V RV32IMC ISA and the Xpulp ISA extensions (i.e., *popcount*, HW loop, post-increment lw/sw) [27]. In Cerutti et al.'s network, the input FM is tiled in 2 tiles with an overlap of 20 columns to fit in the 146 kB FMM. Running these networks on ChewBaccaNN has an actual energy consumption of 1.3/353 μ J/frame, a $585/72 \times$ improvement over the embedded GAP8 implementation (760 mJ and 25.5 J). The highest BNN performance on CIFAR-10 is achieved with Group-Net based on ResNet-18, which reaches 91.5% of accuracy (i.e., 1.5% drop to FP32 baseline) and requires 7.3 μ J.

Furthermore, we evaluate the SoA BNN networks on the challenging ImageNet image classification challenge, whereas this is the first accelerator publishing performance numbers on ImageNet. DoReFa-Net with the smallest reported Top-1 accuracy gap of 12.3% [13], XNOR-Net++ with the best Top-1 accuracy with standard BNNs [28], and the two multi-base binary networks ABC-Net [14] and Zhuang et al. [15]. DoReFa-Net was evaluated with 48 kB FMM, and the others with 76 kB FMM. ABC-Net extends ResNet-18 with 3 parallel BNN layers per original full-precision layer (i.e., 3 weight bases) and reaches an accuracy of 61.0 (-8.3%) requiring 1.12 mJ and Zhuang et al. 67.5 (-1.8%) with $8 \times$ bases with a 3.0 mJ energy cost per frame. XNOR-Net++ can be run at an energy cost of 373 μ J at 61% Top-1 accuracy and a throughput of 23 GOPS.

V. CONCLUSION

We have presented a novel BNN accelerator implemented in GlobalFoundries 22 nm technology, which can perform inference with $2.8 \times$ less energy on CIFAR-10 at the same accuracy than the current state-of-the-art, an analog processing-in-memory device, and $4 \times$ less energy than the next best digital solution which relies on the more recent 10 nm node—all the while providing the option of running also higher accuracy BNNs out of reach of current analog computing architectures. We achieve this by combining a high energy

TABLE II: Real network performance on SoA BNNs. Gap shows the performance difference to the full-precision baseline network

	Acc. %	Gap $\Delta\%$	Util.%	Core Eff. %	Dev. Eff. TOPS/W	P mW	En. μJ	Throughput GOPS	FPS
Freesound , Sound Event Detection with 28 classes, $1 \times 400 \times 64$ MFCC Spectrograms									
[26] $5C^{3 \times 3} - 3C^{1 \times 1}$	77.9	-7.9	37.9	4.2	6.5	2.6	353	16.8	7.2
CIFAR-10 , 10 classes, $3 \times 32 \times 32$									
[24] VGG-like	86.8	-4.6	60.9	36.1	8.2	2.9	1.3	23.9	2286.2
[25] ResNet-18	91.5	-1.5	49.2	24.0	9.2	2.4	7.3	21.8	324.3
ILSVRC , 1'000 classes, $3 \times 224 \times 224$									
[13] AlexNet	43.6	-12.3	45.3	27.8	13.8	2.1	141	28.5	14.7
[28] ResNet-18	57.1	-12.2	52.9	24.7	9.0	2.6	373	23.4	7.0
[14] $3 \times$ ResNet-18	61.0	-8.3	52.9	24.7	9.0	2.6	1,118	23.4	2.3
[15] $8 \times$ ResNet-18	67.5	-1.8	52.9	24.7	9.0	2.6	2,981	23.4	0.9

efficiency of up to 223 TOPS/W, attributable to an efficient on-chip memory hierarchy based on SCMs and strong voltage scaling, with the flexibility to run various filter kernel sizes that allows us to use more efficient BNNs without sacrificing accuracy, thereby boosting the overall energy efficiency beyond what can be measured by the simple TOPS/W metric. Further, we provide the first performance numbers for BNN hardware accelerators on the ILSVRC dataset, as we can run state-of-the-art BNNs such as XNOR-Net++ or Group-Net, reaching a Top-1 accuracy of 61.0% and 67.5% on the ILSVRC'12 dataset at merely 1.1 and 3.0 mJ/frame, respectively.

REFERENCES

- [1] K. He *et al.*, "Deep Residual Learning for Image Recognition," *Proc. IEEE CVPR*, pp. 770–778, 2015.
- [2] A. Khan *et al.*, "A survey of the recent architectures of deep convolutional neural networks," *arXiv preprint arXiv:1901.06032*, 2019.
- [3] V. Sze *et al.*, "Efficient Processing of Deep Neural Networks: A Tutorial and Survey," *Proceedings of the IEEE*, vol. 105, no. 12, pp. 2295–2329, 2017.
- [4] R. Andri *et al.*, "YodaNN: An Architecture for Ultra-Low Power Binary-Weight CNN Acceleration," *IEEE TCAD*, 2017.
- [5] R. Andri *et al.*, "Hyperdrive: A Multi-Chip Systolically Scalable Binary-Weight CNN Inference Engine," *IEEE Journal on Emerging and Selected Topics in Circuits and Systems*, vol. 9, no. 2, pp. 309–322, 6 2019.
- [6] S. Moini *et al.*, "A resource-limited hardware accelerator for convolutional neural networks in embedded vision applications," *IEEE TCAS-II*, 2017.
- [7] L. Cavigelli *et al.*, "Ebpc: Extended bit-plane compression for deep neural network inference and training accelerators," *IEEE JETCAS*, vol. 9, no. 4, pp. 723–734, 2019.
- [8] B. Jacob *et al.*, "Quantization and training of neural networks for efficient integer-arithmetic-only inference," *Proceedings of the IEEE Conference on Computer Vision and Pattern Recognition*, 2018, pp. 2704–2713.
- [9] M. Rastegari *et al.*, "XNOR-Net: ImageNet Classification Using Binary Convolutional Neural Networks," in *Proc. ECCV*, 2016, pp. 525–542.
- [10] I. Hubara *et al.*, "Binarized neural networks," in *Advances in neural information processing systems*, 2016, pp. 4107–4115.
- [11] H. Qin *et al.*, "Binary neural networks: A survey," *Pattern Recogn.*, 2020.
- [12] M. Spallanzani *et al.*, "Additive noise annealing and approximation properties of quantized neural networks," *arXiv preprint arXiv:1905.10452*, 2019.
- [13] S. Zhou *et al.*, "Dorefa-net: Training low bitwidth convolutional neural networks with low bitwidth gradients," *arXiv preprint arXiv:1606.06160*, 2016.
- [14] X. Lin *et al.*, "Towards accurate binary convolutional neural network," in *Advances in Neural Information Processing Systems*, 2017, pp. 345–353.
- [15] B. Zhuang *et al.*, "Structured binary neural networks for accurate image classification and semantic segmentation," in *Proceedings of the IEEE Conference on Computer Vision and Pattern Recognition*, 2019, pp. 413–422.
- [16] F. Conti *et al.*, "XNOR Neural Engine: A Hardware Accelerator IP for 21.6-fJ/op Binary Neural Network Inference," *IEEE Transactions on Computer-Aided Design of Integrated Circuits and Systems*, vol. 37, no. 11, pp. 2940–2951, 2018.
- [17] J. Lee *et al.*, "Unpu: An energy-efficient deep neural network accelerator with fully variable weight bit precision," *IEEE Journal of Solid-State Circuits*, vol. 54, no. 1, pp. 173–185, 2018.
- [18] D. Bankman *et al.*, "An Always-On 3.8 uJ/86% CIFAR-10 Mixed-Signal Binary CNN Processor With All Memory on Chip in 28-nm CMOS," *IEEE Journal of Solid-State Circuits*, vol. 54, no. 1, pp. 158–172, 2018.
- [19] P. C. Knag *et al.*, "A 617 tops/w all digital binary neural network accelerator in 10nm finfet cmos," in *2020 IEEE Symposium on VLSI Circuits*. IEEE, 2020, pp. 1–2.
- [20] H. Valavi *et al.*, "A 64-tile 2.4-mb in-memory-computing cnn accelerator employing charge-domain compute," *IEEE Journal of Solid-State Circuits*, vol. 54, no. 6, pp. 1789–1799, 2019.
- [21] A. Al Bahou *et al.*, "XNORBIN: A 95 Top/s/W hardware accelerator for binary convolutional neural networks," in *21st IEEE Symposium on Low-Power and High-Speed Chips and Systems, COOL Chips 2018 - Proceedings*, 2018, pp. 1–3.
- [22] Y. Bengio *et al.*, "Estimating or propagating gradients through stochastic neurons for conditional computation," *arXiv preprint arXiv:1308.3432*, 2013.
- [23] B. Moons *et al.*, "BinarEye: An always-on energy-accuracy-scalable binary CNN processor with all memory on chip in 28nm CMOS," in *2018 IEEE Custom Integrated Circuits Conference (CICC)*. IEEE, 2018, pp. 1–4.
- [24] M. Rusci *et al.*, "Always-ON visual node with a hardware-software event-based binarized neural network inference engine," in *2018 ACM International Conference on Computing Frontiers, CF 2018 - Proceedings*. ACM, 2018, pp. 314–319.
- [25] H. Qin *et al.*, "Forward and backward information retention for accurate binary neural networks," in *Proceedings of the IEEE/CVF Conference on Computer Vision and Pattern Recognition*, 2020, pp. 2250–2259.
- [26] G. Cerutti *et al.*, "Sound Event Detection with Binary Neural Networks on Tightly Power-Constrained IoT Devices," in *ISLPED*. ACM/IEEE, 2020.
- [27] M. Gautschi *et al.*, "Near-Threshold RISC-V core with DSP extensions for scalable IoT endpoint devices," *IEEE TVLSI*, vol. 25, no. 10, pp. 2700–2713, 2017.
- [28] A. Bulat and G. Tzimiropoulos, "XNOR-Net++: Improved binary neural networks," *arXiv preprint arXiv:1909.13863*, 2019.